Supercritical Gas–Polymer Interactions with Applications in the Petroleum Industry. Determination of Thermophysical Properties

Séverine A. E. Boyer,[1] Marie-Hélène Klopffer,[2] Joseph Martin,[3] Jean-Pierre E. Grolier[1]

[1]*Laboratory of Thermodynamics of Solutions and Polymers, Clermont–Ferrand, Blaise Pascal University, 63 177 Aubière Cedex, France*
[2]*French Institute of Petroleum, Paris, 92 852 Rueil-Malmaison Cedex, France*
[3]*French Institute of Petroleum, Lyon, 69 390 Vernaison Cedex, France*

Received 17 January 2006; accepted 22 May 2006
DOI 10.1002/app.25085
Published online in Wiley InterScience (www.interscience.wiley.com).

ABSTRACT: The knowledge of chemical equilibria in {gas–polymer} systems plays an essential role as regards the safety of transport of petroleum products in polymer-made pipes. Thermophysical properties of thermoplastic semicrystalline polymers are key data for the development of several engineering applications. These applications require the investigation of the behavior of a polymer, in the solid state i.e., between glass-transition temperature T_g and melting-transition temperature T_m, submitted to the triple thermal, barometric, and chemical constraint. The chemical stress results from supercritical fluid sorption. The relatively high temperature and pressure, industrial operating conditions, require for laboratory investigations the use of sophisticated experimental instrumentation in which such extreme conditions can be reproduced. In this context, coupling gas solubility and swelling techniques (VW-*PVT*) on the one hand, calorimetry and *PVT* techniques (*P*CSC) on the other hand, over extended temperature and pressure ranges, provide a wide spectrum of thermophysical and thermomechanical properties like solubility and isobaric thermal expansion, in absence or in presence of solubilized gases. Selected examples taken in the petroleum industry, dealing with different polymers [medium density polyethylene, poly (vinylidene fluoride)] in presence of gases (carbon dioxide CO_2, nitrogen N_2), serve to illustrate the importance of gas solubility (VW-*PVT*) (Boyer and Grolier, Polymer 2005, 46, 3737) data and of heats of interaction (*P*CSC) measurements (Randzio et al., Fr. Pat. 9109227, Pol. Pat. 295285; Randzio, Chem Soc Rev 1996, 25, 383; Boyer et al., J Polym Sci Part B: Polym Phys 2006, 44, 185) in the broad field of applied polymer thermodynamics. © 2006 Wiley Periodicals, Inc. J Appl Polym Sci 103: 1706–1722, 2007

Key words: supercritical gases; semicrystalline polymers; thermophysical properties; vibrating-wire sensor; pressure-controlled scanning calorimetry

INTRODUCTION

Organic macromolecular materials, i.e., polymers, are very often in contact with supercritical fluids in petroleum applications, either as on-duty materials (containers, pipes) or as process intermediates (foaming, molding). To better improve or control the use and life-time of end products made of such polymers, to adequately preserve the environment and safely transport fluids, knowledge of the thermophysical properties of polymers over extended ranges of temperatures and pressures in different gaseous environments is of paramount necessity. In particular, in the petroleum industry, the transport of petroleum fluids is made using flexible hosepipes, whose structures contain extruded thermoplastic or rubber sheaths and reinforcing metallic armor layers. Depending on the type of transported fluids, their acidity, operating temperature, and pressure of the extraction, polyethylene (PE), polyamide (PA), and poly(vinylidene fluoride) (PVDF or PVF_2) composed the sheaths. But these thermoplastic polymers, like elastomers, are not entirely impermeable and undergo sorption/diffusion phenomena. A rupture of the thermodynamic equilibrium after a sharp pressure drop may eventually damage polymer components. Gas concentration in the polymer, with temperature gradients, causes irreversible ''explosive'' deterioration of the polymeric structures. This process manifests itself by cracks, blisters, or microstructures-like foams (Fig. 1). This blistering phenomenon is usually termed as ''explosive decompression failure'' (XDF).[1,2–4] The resistance to physical changes is related to the influence of the different interactions on the thermophysical properties of the polymer. The estimation of the gas sorption and of the concomitant polymer swelling as well as the measurement of the thermal effect associated with the gas–polymer interactions provide valuable and basic information for a better understanding of the polymer behavior in different applications, where temperature and pressure, in com-

Correspondence to: M.-H. Klopffer (M-Helene.Klopffer@ifp.fr) or J. Martin (Joseph.Martin@ifp.fr) or J.-P. E. Grolier (J-Pierre.Grolier@univ-bpclermont.fr).

Journal of Applied Polymer Science, Vol. 103, 1706–1722 (2007)

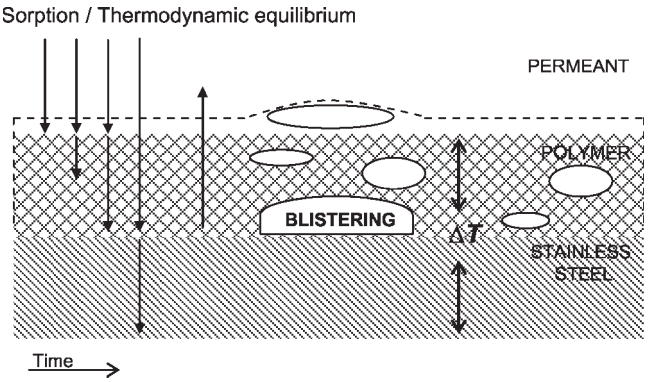

Figure 1 Representation of the blistering phenomenon or ''explosive decompression failure'' (XDF). Under gas pressure, the polymer becomes saturated in the gas at the thermodynamic equilibrium. Following a pressure drop, gas concentration in the polymer together with temperature gradients causes irreversible ''explosive'' deterioration of the polymeric structures. Cracks, blisters, or microstructures-like foams can appear.

bination with supercritical fluid stress, may deeply affect the polymer stability and properties.[5–14]

In the present article, we report two complementary thermodynamic approaches to characterize gas–polymer interactions in evaluating either gravimetric and volumetric changes or thermally energetic changes associated to gas sorption (up to saturation) in polymer. The first approach is based on a ''weighing technique'' using a vibrating-wire (VW) sensor, coupled with a *PVT* method.[1,15–17] Investigations concern the interactions of carbon dioxide (CO_2) with two polymers, medium-density polyethylene (MDPE) {CO_2–MDPE} and poly(vinylidene fluoride) (PVDF) {CO_2–PVDF}, during sorption (CO_2-pressurization)/desorption (CO_2-depressurization). The second approach consists of measuring heat fluxes due to gas–polymer interactions. Calorimetric investigations were carried with pressure-controlled scanning calorimetry (*P*CSC), and different detection modes were developed.[18,19] Qualitative and quantitative analyses of interactions of medium-density polyethylene (MDPE) and poly (vinylidene fluoride) (PVDF) with carbon dioxide (CO_2) and nitrogen (N_2) during sorption/desorption have been made along isotherms, under pressure jumps, as well as under pressure and volume scans. Furthermore, the two polymers have been compared to each other directly in the same gaseous environment under identical thermodynamic conditions.

EXPERIMENTAL TECHNIQUES

''Weighing-*PVT*'' methodology: Sorption and swelling

As described previously,[1,15–17] VW-*PVT* is a methodology developed to simultaneously calculate the concentration of a gas in the polymer and the volume change of the polymer during the sorption by means of two rigorous working equations. The vibrating-wire (VW) sensor is used as a ''weighing technique,'' while the *PVT* method (three-cell principle) permits a series of successive transfers of the gas by connecting the calibrated transfer cell V_3 to the equilibrium cell V_2 that contains the polymer (Fig. 2).

In the working equation of the VW sensor, the mass m_{sol} of gas dissolved into the polymer is related to the change in volume ΔV_{pol} of the polymer due to sorption as shown by the eq. (1) and the volume of the degassed polymer is represented by V_{pol}.

$$m_{sol} = \rho_g \, \Delta V_{pol} + \left[(\omega_B^2 - \omega_0^2) \frac{4 \, L^2 \, R^2 \, \rho_s}{\pi \, g} + \rho_g \, (V_C + V_{pol}) \right] \quad (1)$$

All parameters have a physical meaning: ω_0 and ω_B represent the natural angular frequencies of the wire in vacuum and under pressure, respectively; V_C the volume of the container; L, R, and ρ_s are the length, radius, and density of the wire, respectively; and ρ_g the density of the fluid. The container, where the polymer sample is seated, is suspended to the vibrating wire in the measuring cell. The natural angular frequency of the wire depends on the change of weight (and volume) of the polymer sample during gas sorption and it is then directly related to the amount of gas absorbed.

In the working equation of the *PVT* method, the amount of gas absorbed by the polymer sample, after successive transfers once equilibration is attained, is related to the change in volume ΔV_{pol} of the polymer as shown by the eq. (2).

$$\Delta m_{sol}^{(k)} = \frac{M_g}{R} \frac{P_f^{(k)} \Delta V_{pol}^{(k)}}{Z_f^{(k)} T_f^{(k)}} + \frac{M_g}{R} \left[\frac{P_i^{(k)} V_3}{Z_i^{(k)} T_i^{(k)}} + \frac{P_f^{(k-1)} \left(V_2 - V_{pol} - \Delta V_{pol}^{(k-1)} \right)}{Z_f^{(k-1)} T_f^{(k-1)}} - \frac{P_f^{(k)} \left(V_2 + V_3 - V_{pol} \right)}{Z_f^{(k)} T_f^{(k)}} \right] \quad (2)$$

M_g is the molar mass of the dissolved fluid, Z_i and Z_f are the compression factors of the gas entering the polymer respectively, at the initial (index *i*) and final (equilibrium sorption, index *f*) conditions. $\Delta m_{sol}^{(k)}$ is the increment in mass of absorbed gas after the transfer k and $\Delta V_{pol}^{(k)}$ is the associated change in volume after transfer k.

Both eqs. (1) and (2) can be written in the same form [eq. (3)] because of the common expression of density of the gas ρ_g given by $\rho_g = \frac{M_g}{R} \frac{P_f}{Z_f T_f}$

$$\Delta m_{sol}^{(k)} = \rho_g \, \Delta V_{pol} + d \quad (3)$$

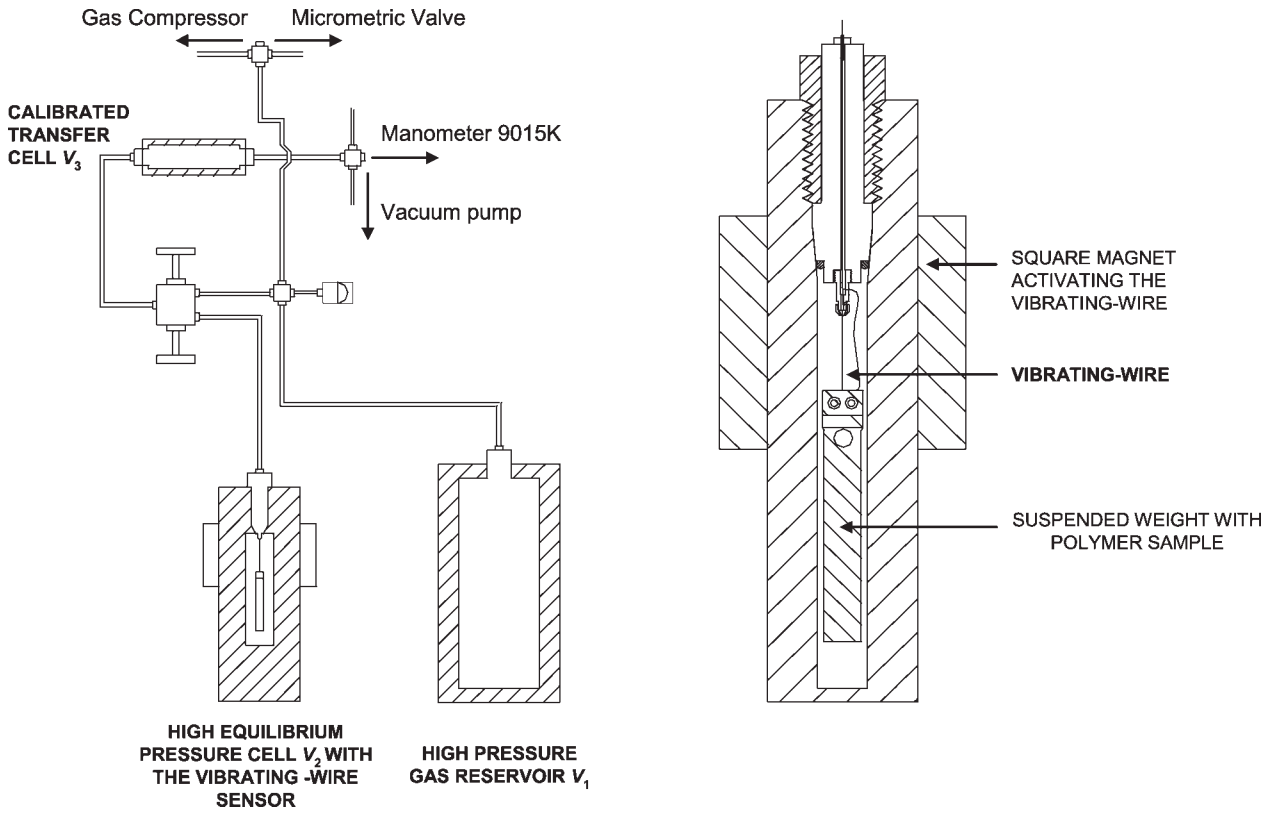

Figure 2 Schematic view of the VW-*PVT* set-up. On the left hand side is the three-cell principle for *PVT* measurements. On the right hand side is the representation of the ''weighing vibrating-wire sensor.'' The polymer sample seats in the container, which is suspended to a thin tungsten vibrating-wire (25 μm, 0.03 m) in the measuring cell. The natural angular frequency of the wire depends on the amount of gas absorbed.

d represents the apparent concentration of gas in the polymer, i.e., when the change in volume ΔV_{pol} is zero. The volume change ΔV_{pol} and the total mass of dissolved gas m_{sol} are the unknown terms.

Since the *PVT*-technique may generate cumulative errors whereas the vibrating-wire technique does not require extensive calibrations, the VW sensor technique is then considered to be more precise. A detailed description of the technique was given in Ref. 1. Because of the similar writing of eqs. (1) and (2) through eq. (3), the swelling data of the polymer during sorption are calculated through data obtained using a theoretical model. For this, the Sanchez–Lacombe equation of state SL-EOS[20–22] [eqs. (4) and (5)] together with the equation of DeAngelis[23] [eq. (6)] were selected. Estimation of the change in volume of the polymer was made with the SL-EOS, in which only one binary adjustable interaction parameter k_{12} has to be calculated by fitting the sorption data:

$$\Delta p^* = k_{12}\sqrt{P_1^* P_2^*} \tag{4}$$

$$\omega_1 = \frac{\phi_1}{\phi_1 + (1-\phi_1)\frac{\rho_2^*}{\rho_1^*}} \tag{5}$$

where Δp^* is the parameter characterizing the interactions in the mixture, ω_1 is the mass fraction of permeant gas at equilibrium, ϕ_1 is the volume fraction of the gas in the polymer, (ρ_1^*, P_1^*, T_1^*) and (ρ_2^*, P_2^*, T_2^*) are the characteristic parameters of pure compounds;

$$\frac{\Delta V_{\text{pol}}}{V_{\text{pol}}} = \frac{1}{\tilde{\rho}\rho^*(1-\omega_1)}\frac{1}{\hat{v}_2^0} \tag{6}$$

where ρ^* and $\tilde{\rho}$ are respectively, the mixture characteristic and reduced densities, and $\hat{v}_2^0$ is the specific volume of the pure polymer at fixed temperature T, pressure P, and composition.

According to the procedure, the solubility data are obtained through combined experimental measurements and theoretical estimation of the volume change of the polymer due to the sorption.

''Calorimetry-*PVT*'' methodology: Thermophysical properties

In a previous work,[18] a new experimental and theoretical approach has been proposed to study transitions in {gas–polymer} systems in terms of heat involved. Scanning transitiometry, which combines a calorimetric detector with a *PVT* scanning technique, offers

advantageous features for such study. The differential mode of operation permits to control precisely both temperature T and pressure P keeping them exactly identical in the two calorimetric (reference and measuring) cells.[24,25] The PVT technique allows to scan pressure P or volume V during sorption (fluid-pressurization) and desorption (fluid-depressurization). The calorimetric detector measures the differential heat flux (between reference and measuring cells) resulting from the physicochemical effects occurring during the sorption/desorption runs. From the determination of the heat involved in the measuring cell (containing the polymer sample) and by virtue of the Maxwell's relation, $(\partial S/\partial P)_T = -(\partial V/\partial T)_P$, the global cubic thermal expansion coefficient of the gas-saturated polymer $\alpha_{\text{pol-g-int}}$ is obtained at different isothermal conditions, as shown by [eq. (7)]

$$\alpha_{\text{pol-g-int}} = \frac{\left(Q_{\text{diff,SS}} - Q_{\text{diff,pol}}\right) + V_{\text{SS},r}\ \alpha_{\text{SS}}\ T\ \Delta P}{V_{\text{pol}}\ T\ \Delta P} \quad (7)$$

Q_{pol} and Q_{ss} represent the heat fluxes corresponding to the polymer sample and to the inert sample (made of stainless steel) respectively, placed in the measuring and reference cells, α_{ss} is the cubic expansion coefficient of the stainless steel which are made of the cells, and ΔP the variation of gas-pressure change under investigation at constant temperature T. V_{ss} with V_{pol} are the volumes of the stainless steel inert reference and of the polymer. In eq. (7), it was assumed for simplicity ''*faute de mieux*'' that the volume of the polymer did not change significantly upon gas sorption. This assumption may be justified in the sense that in calorimetric measurements, pressure is much higher ($\sim$ 100 MPa) than that in the case of the VW-PVT technique ($\sim$ 40 MPa); the hydrostatic pressure must probably compensate for a large part of the swelling effect due to gas sorption, as a result of the equilibrium between plasticization effect and hydrostatic effect (see paragraph Results and Discussion, Thermophysical properties).

Essentially three differential modes were investigated taking into account the differential principle of the instrument (Fig. 3): thermal I differential without reference sample, thermal II differential with reference sample, and thermal II differential comparative mode. With the thermal I differential mode, in an initial experiment, the polymer sample was placed in the measuring cell that is connected to the gas line. The reference cell, not connected to the gas line, was acting as a thermal reference. An additional blank experiment (under identical conditions) was performed by replacing the polymer sample by an inert-metal (stainless steel) sample of similar volume. Then, the difference of the heat effects between polymer and blank experiments allowed to quantify the thermal effect due to the gas–polymer interactions. In the thermal II differential mode, the polymer sample was placed in the measuring cell, while an inert-metal sample of equal dimensions was seated in the reference cell, both cells being connected to the gas line, which serves to pressurize. Then, under gas pressure, the calorimetric differential signal is proportional to the thermal effect due to the gas–polymer interactions. The third and last mode corresponds to a validation of the two previous modes through the thermal II dif-

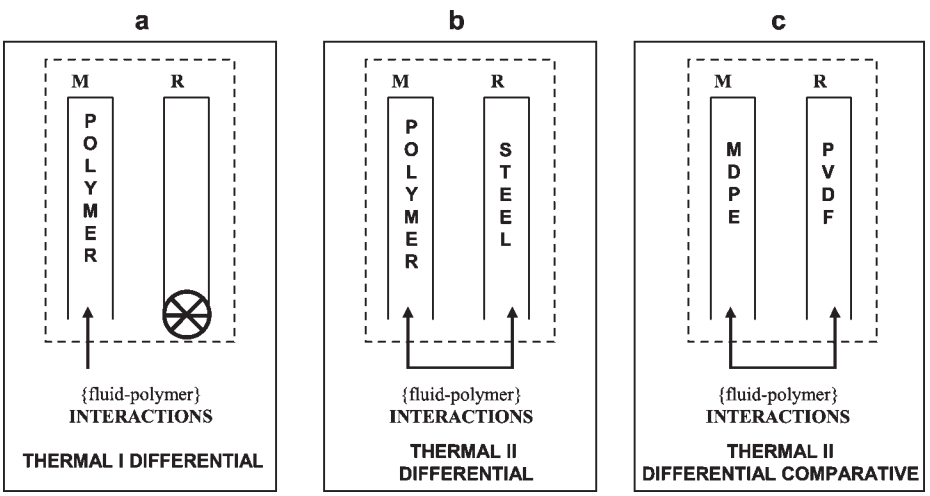

Figure 3 Scanning transitiometry with three differential modes according to the differential principle of the calorimetric detector, taking into account the respective role of the measuring M and reference R cells and regarding the content of the reference cell. (a) Thermal I differential without reference sample mode, where the measuring cell contains the polymer or the inert sample in contact with the gas, while the reference acts as a thermal reference; (b) Thermal II differential with reference sample mode, where the measuring cell contains the polymer sample, while the reference cell contains an inert sample of equal volume, both cells being connected to the gas line; (c) Thermal II differential comparative mode, where the measuring cell contains the MDPE sample, while the reference cell contains the PVDF sample, both cells being connected to the same gas line.

ferential comparative mode, firstly described and employed by us. This allows to directly compare the response and behavior of two polymer samples, MDPE and PVDF, in similar supercritical conditions. A MDPE polymer sample was placed in the measuring cell, while a PVDF polymer sample of equal size and volume was placed in the reference cell. Both cells were connected to the gas line. The calorimetric signal, i.e., the differential heat flux, was thus directly proportional to the thermal effect due to the difference of the gas–polymer interactions between the two polymers interacting with the same gas. In that case, the differential heat flux between both measuring and reference cells is small, because calorimetric signals of {gas–MDPE} and {gas–PVDF} systems have relatively close amplitudes; the detection sensitivity of the apparatus was then optimal. For each thermal II differential with reference sample and thermal II differential comparative mode, the data have been corrected through a blank standard calibration. Under identical conditions of T and P, and under the assumption that there were no interactions between the metal-stainless steel rod and the gas, blank experiments were performed by replacing the polymer samples by a metal sample of identical dimensions.

Materials and experimental set-up

Polymers investigated are main components, as efficient barriers against light fluids, for making on-duty materials used for the transport of fluids (pipe-lines, seals). Investigation of the polymer behavior consists typically in measuring the physicochemical properties in the solid state, i.e., between glass-transition temperature T_g and melting-transition temperature T_m. Medium-density polyethylene (MDPE) and poly(vinylidene fluoride) (PVDF) were submitted to gas pressure of either carbon dioxide (CO_2) or nitrogen (N_2) at different temperatures comprised between 333 and 403 K, under pressure steps or scans in the range between 0.1 and 100 MPa. Extruded MDPE (reference Finathene 3802) and PVDF (reference Kynar 50HD, polymer without additives like plastifiants or elastomers) was supplied by the French Institute of Petroleum (Institut Français du Pétrole, IFP). The transitions temperatures T_g and T_m for MDPE are 163.0 and 400.0 K and for PVDF are 235.0 and 440.9 K, respectively (Table I). Values of T_g were given by IFP. Values of T_m, for the two polymers having respectively, the degrees of crystallinity X_c, 49 and 48%, were determined from the measurements of the enthalpies of fusion of semicrystalline polymers ΔH_{fc}. A temperature modulated-differential scanning calorimeter [Mettler-Toledo] TMDSC type 821e was used. Modulation of temperature parameters were: temperature rate $q_{TMDSC} = 2.00$ K min^{-1}, amplitude of modulation of temperature $A_T = 0.8$ K min^{-1}, and period of modulation $p_{TMDSC} = 60$ s. The mass of sample was about 2–5 mg and thermograms were obtained under a continuous flow of nitrogen at a rate of 15 mL min^{-1}. The extrapolated onset temperature was assigned to the melting temperature. The degrees of crystallinity X_c were calculated from the fusion enthalpy of a 100% crystalline polymer $\Delta H_{f100\%\ c}$ taken from literature, with respectively, 293.014 J g^{-1} for PE sample and 104.631 J g^{-1} for PVDF sample [site http://web.utk.edu/].

Different geometries of polymer samples were used according to the experimental set-up. In the case of VW-*PVT*, measurements with MDPE were performed at 333.15 and 338.15 K on a set of thin rods (length 65.0 mm, diameter 2.1 mm) having a total mass around 3.750 g. Measurements with PVDF were performed at 391.15 K either on a set of circular cross section rods (length 58.1 mm, diameter 2.4 mm) having a total mass of 5.716 g, or on a single rectangular cross section rod sample (length 69.9 mm, width 8.8 mm, thickness 5.1 mm) having a total mass of 5.588 g. In the case of pressure scanning calorimetry, the measurements were performed on cylindrical rod samples (75.0 mm in height, 4.4 mm in diameter) having a rela-

TABLE I
Thermophysical Properties of Native Polymers (MDPE, PVDF) and Fluids (CO_2, N_2)

Polymers	MD polyethylene (MDPE)	Poly(vinylidene fluoride) (PVDF)
Glass-transition, T_g (K)	163.0	235.0
Melting-transition, T_m (K)	400.0	440.9
Crystallinity, X_c (%)	49	48
Crystallinity,[7] X_c (%)	51	50
Fluids	**Carbon dioxide (CO_2)**	**Nitrogen (N_2)**
Purity (%)	99.50	99.95
Humidity, T_c (%)	< 10	
Critical temperature, P_c (K)	304.130	126.193
Critical pressure, M_g (MPa)	7.37521	3.39780
Molar mass (g mol^{-1})	44.0098	28.013

tively small mass, i.e., about 1.0 g for MDPE sample and 1.9 g for PVDF sample; measurements were taken from 352.38 to 401.50 K. For each investigation, a new sample was used.

Both gases, carbon dioxide CO_2 (purity of 99.5%) and nitrogen N_2 (purity of 99.95%), were supplied by SAGA France and used without further purification. The critical points (P_c and T_C) are, respectively, for CO_2 7.38 MPa and 304.13 K, and for N_2 3.40 MPa and 126.19 K (Table I). The two gases were selected for their different properties: essentially N_2 being less polar than CO_2 is considered as more ''neutral'' when interacting with polymers. Mercury (Hg) was used as a chemical inert pressure transmitting fluid and preferred due to its well-known thermomechanical coefficients ($\alpha_P = 1.80 \times 10^{-4}\,K^{-1}$ and $\kappa_T = 0.40 \times 10^{-4}\,MPa^{-1}$).

RESULTS AND DISCUSSION

Gravimetric–volumetric properties

In this section, we report the experimental VW-*PVT* measurements and the calculation of the apparent concentration of CO_2 associated to the swelling of the polymer, calculated using the Sanchez–Lacombe equation of state (SL-EOS).

Sorption of CO_2 in MDPE

The apparent concentration d of CO_2 in MDPE at 333.15 and 338.15 K is first represented Figure 4. A comparison of the behavior of PE at high pressure in the solid and molten states is possible with the work of Flaconnèche et al.,[26] Chaudary and Johns,[10] and Sato et al.[11] Flaconnèche et al. have studied MDPE by using a gravimetric method. Chaudary and Johns have studied LDPE by using a gravimetric magnetic suspension device (MSD). Sato et al. have studied HDPE by using a pressure decay method. As expected, the concentration in the molten state is higher compared to the concentration in the solid state.

The corrected concentration of CO_2 in MDPE takes into consideration the volume change of the system [eqs. (5) and (6), Figs. 5 and 6, Table II]. At 333.15 K and 35 MPa, the calculated volume change is 4%, whereas at 338.15 K and 21 MPa it is 2.5%. The data are close to those obtained previously at IFP.[27] In Figures 5 and 6, an other direct comparison is made with the results of Kamiya et al.[9] obtained for low-density polyethylene LDPE in interaction with CO_2 using a gravimetric method up to 5 MPa at 308.15 K. Polymer swelling as well as gas concentration in polymer sample increase with pressure and tend to level off.

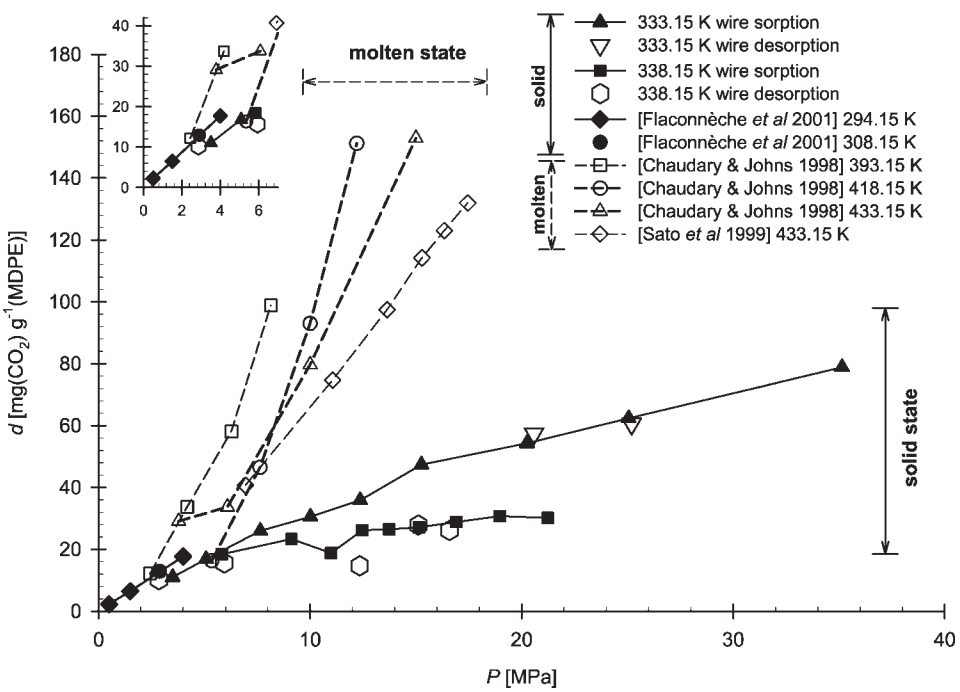

Figure 4 Representation of the apparent concentration d [eq. (3)] of CO_2 in MDPE calculated from solubility data obtained with the vibrating wire sensor VW at 333.15 and 338.15 K (parameters of supercritical CO_2: $T_c = 304.13$ K, $P_c = 7.375$ MPa, $\rho_c = 467.816$ kg m^{-3}). Comparison of results obtained under either sorption or desorption with solid MDPE. Values of d for solid MDPE are smaller than that for molten PE. Comparison with literatures: [Flaconnèche et al., 2001 with MDPE, using a gravimetric method[26]], [Chaudary and Johns, 1998 with LDPE, using a magnetic suspension device[10]], and [Sato et al., 1999 with HDPE, using a pressure decay method[11]]. The low pressure region (7 MPa) is represented in the inset.

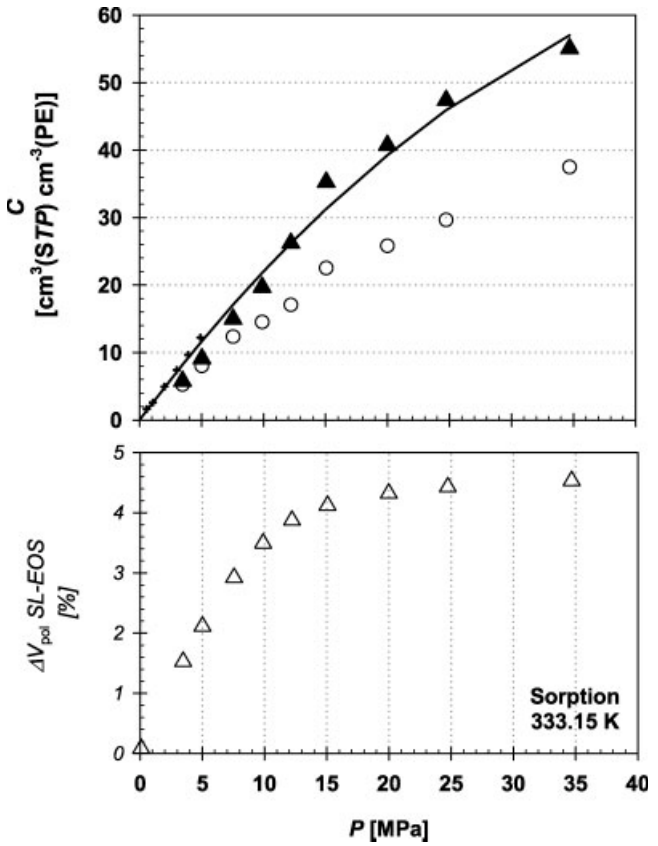

Figure 5 Sorption of CO_2 up to 35 MPa in MDPE at 333.15 K as a function of pressure. Apparent concentrations are represented with open circles. Corrected concentrations (closed triangles) were calculated taking into account the swelling ΔV_{pol} of the polymer (ΔV_{pol} values estimated using SL-EOS are represented with open triangles in lower graph). Full line represents the ''dual-mode'' model fitting of the corrected values. Comparison with literature: [+, Kamiya et al., 1986 with LDPE at 308.15 K, using a gravimetric method[9]].

Solubility data obtained at higher temperature are smaller. CO_2 sorption is found to be well-correlated with the ''dual-mode'' sorption model[1,5,28–37]; the corresponding parameters are listed in Table IV. Data obtained during both sorption and desorption are in good agreement.

Sorption of CO_2 in PVDF

In the same manner, the apparent and corrected concentrations of CO_2 in PVDF at 391.15 K are shown in Figure 7 and listed in Table III. The apparent curve shows a maximum near 10 MPa with a value of 18 cm^3 (standard temperature and pressure; STP) cm^{-3} (PVDF). This trend was observed with two independent studies: it shows first the reliability of the apparatus, second the noninfluence of the geometry of the sample on the gas concentration when the system is at the thermodynamic equilibrium. It is worth-noting that this trend is attributed to the under-estimation of the polymer swelling.[1,38] By means of SL-EOS, a volume change of 14% was determined at 42 MPa. At pressure up to 10 MPa, neglecting swelling does not affect the solubility, but around 15 MPa the volume change seems to become larger. The last observation agrees with the results of Lorge et al.[39] who performed dilatation studies for the {CO_2–PVDF} system at 353.15 K using an ultrasonic transducer. Our corrected data were correlated with the ''dual-mode'' model; the corresponding parameters are listed in Table IV.

Conclusion: Sorption of CO_2 in MDPE and PVDF

The results show that CO_2 sorption is higher in PVDF than in MDPE. Both polymers having the same volume fraction of amorphous state, $\phi_a = 0.53$,[1,7] solubility is favored by the presence of polar groups C—F in the PVDF main chain.[40,41] This is shown by CO_2–PVDF interactions that are stronger than CO_2–MDPE interactions. The extent of the gas–polymer interac-

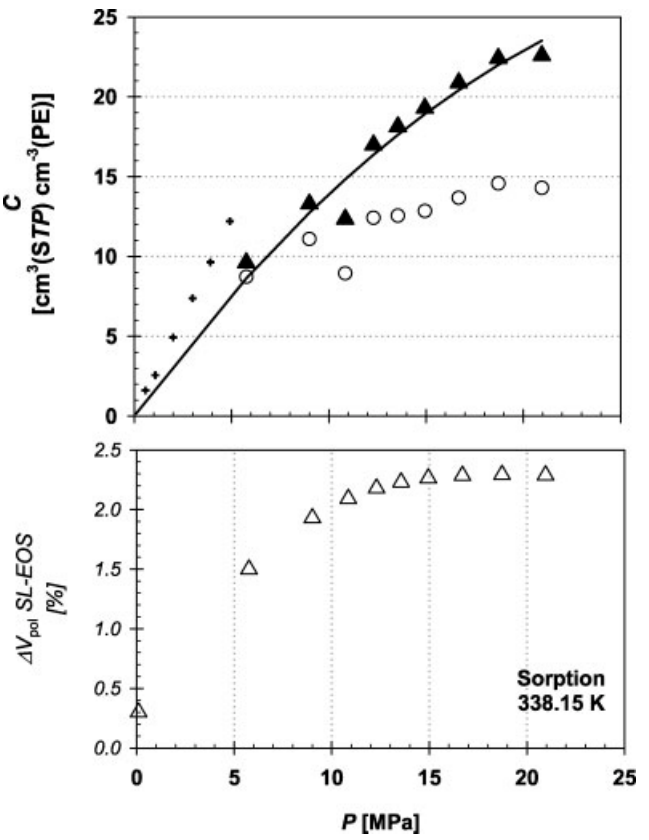

Figure 6 Sorption of CO_2 in MDPE at 338.15 K, as a function of pressure up to 21 MPa. Apparent concentrations are represented with open circles. Corrected concentrations (closed triangles) were calculated taking into account the swelling ΔV_{pol} of the polymer (ΔV_{pol} values estimated using SL-EOS are represented with open triangles in lower graph). Full line represents the ''dual-mode'' model fitting of the corrected values. Comparison with literature: [+, Kamiya et al., 1986 with LDPE at 308.15 K, using a gravimetric method[9]].

TABLE II
Corrected Concentrations *C* of CO_2, Obtained Using the Vibrating-Wire Sensor, in MDPE, at 333.15 and 338.15 K during Sorption and Desorption under Different Pressures

	P at 333.15 K (MPa)	$C_{corrected}$ VW [cm^3(STP) cm^{-3}(polymer)]	*P* at 338.15 K (MPa)	$C_{corrected}$ [cm^3(STP) cm^{-3}(polymer)]
Sorption	3.51	5.74	5.84	9.61
	5.09	9.07	9.12	13.29
	7.65	14.95	10.99	12.34
	10.02	19.68	12.46	16.99
	12.37	26.19	13.73	18.12
	15.26	35.22	15.14	19.29
	20.25	40.71	16.91	20.89
	25.06	47.38	18.97	22.41
	35.14	55.04	21.23	22.59
Desorption	25.20	46.94	16.59	18.26
	20.58	43.08	15.12	20.05
			12.35	11.44
			5.95	8.31
			2.86	5.22

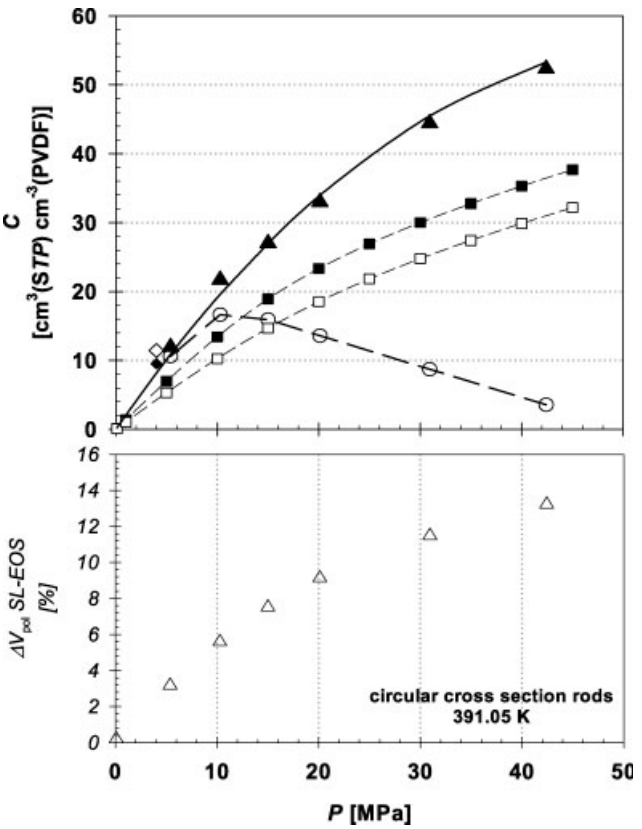

Figure 7 Sorption of CO_2 in PVDF circular cross section rods at 391.05 K as a function of pressure up to 43 MPa. Apparent concentrations are represented with open circles. Corrected concentrations (closed triangles) were calculated using the change in volume of the polymer estimated using the SL-EOS (values represented with open triangles in lower graph). Full line represents the ''dual-mode'' model fitting of the corrected concentrations. [Data of Rodgers at 373.15 K are represented with closed squares and at 398.15 K with open squares, respectively.[38] Data of Flaconnèche et al. on PVF_2 are represented at 370.13 and 404.13 K with closed and open diamonds, respectively.[7]]

tions can be completed and well-documented through thermophysical properties of gas-saturated polymers by means of thermal analysis.

Thermophysical properties

In this section, we present the experimental high-pressure calorimetric measurements. The pressure effect of different pressurizing fluids is determined and allows comparison between polymers, using isotherms of $\alpha_{pol\text{-}g\text{-}int}$ coefficients as well as thermal energies of interactions.

The thermal II differential mode with reference sample: MDPE and PVDF samples at 352 and 372 K under pressure jumps

The first study concerns pressure changes of CO_2 and N_2 at 352.38 and 372.02 K, under pressure jumps of

TABLE III
Corrected Concentrations *C* of CO_2, Obtained Using Vibrating-Wire Sensor, in PVDF Around 391.15 K during Sorption under Different Pressures with Two Different Types of Samples

T (K)	*P* (MPa)	$C_{corrected}$ [cm^3(STP) cm^{-3}(polymer)]
391.05 Sorption circular cross section rods	5.47	11.94
	10.43	21.71
	15.20	27.02
	20.38	32.99
	31.34	44.42
	42.97	52.34
391.50 Sorption rectangular cross section rod	5.36	13.65
	10.63	24.00
	19.64	37.04
	29.75	49.23
	42.70	59.12

TABLE IV
Coefficients Obtained by Fitting the Experimental Data with the Two Correlating Models: Adjustable k_{12} Parameters Used with the SL-EOS and Parameters (k_D, C'_H, b) Used with the "Dual-Mode" Model, Respectively

	SL-EOS, $\Delta p^* = k_{12}\sqrt{P_1^* P_2^*}$	"Dual-mode" model, $C = C_D + C_H = k_D P + C'_H \frac{bP}{1+bP}$		
	k_{12}	k_D [cm^3(STP) cm^{-3}(polymer)$^{-1}$ P^{-1}]	C'_H [cm^3(STP) cm^{-3}(polymer)]	b (atm^{-1})
MDPE 333.15 K				
Sorption	0.8600	−0.375	1403	0.0004
Desorption	0.8603	−0.375	1403	0.0004
MDPE 338.15 K				
Sorption	0.8070	−0.0826	162.3	0.0015
Desorption	0.8060	−0.0826	162.3	0.0015
PVDF 391.15 K				
Sorption	0.9450	−0.375	1403	0.0004

6–28 MPa in the pressure range between 0.1 and 100 MPa (Tables V–VII). CO_2-pressurizing pressure jumps manifest themselves by exothermic heat fluxes,[18,19] while CO_2-depressurization pressure jumps exhibit endothermic heat fluxes, both passing through a minimum around 20 MPa. Interestingly, the heat flux minimum is reflected on the isotherms of $\alpha_{\text{pol-g-int}}$ coefficients of the fluid-saturated polymers plotted as functions of the feed pressure. The global cubic thermal expansion coefficients $\alpha_{\text{pol-g-int}}$ of saturated polymer were obtained through the procedure previously described.[18] Comparison of these coefficients for both polymers (MDPE and PVDF) under CO_2 and N_2, which is the corresponding curves for the {CO_2–MDPE}, {CO_2–PVDF}, and {N_2–PVDF} systems, show a clear a difference (Fig. 8). Additional investigations of {Hg–MDPE} and {Hg–PVDF} systems have been made using mercury as an "inert" pressure transmitting fluid.[18,42] High Hg-pressure runs permit to decouple hydrostatic pressure effects from solvent solubility effects, whereas high N_2-pressure runs permit to separate the preferential interaction effects between polymers with respect to CO_2. Under CO_2, $\alpha_{\text{pol-g-int}}$ shows minima around 14–18 and 21–25 MPa, respectively, for MDPE and PVDF, in contrast to what is observed

TABLE V
Global Cubic Thermal Expansion Coefficients $\alpha_{\text{pol-g-int}}$ at 352.38 K Obtained by Transitiometry with the Thermal II Differential with Reference Sample Mode for MDPE and PVDF Saturated with CO_2

	P (MPa)	Global $\alpha_{\text{pol-g-int}}$ (K^{-1})
{CO_2-MDPE} sorption	3.0 ± 0.1	(1.10 ± 0.03) × 10^{-3}
	8.7 ± 0.1	(7.11 ± 0.20) × 10^{-4}
	14.1 ± 0.1	−(3.99 ± 0.11) × 10^{-5}
	21.4 ± 0.1	(2.84 ± 0.07) × 10^{-4}
	30.3 ± 0.1	(6.96 ± 0.18) × 10^{-4}
	40.5 ± 0.1	(7.19 ± 0.18) × 10^{-4}
	52.9 ± 0.1	(9.83 ± 0.27) × 10^{-4}
	69.4 ± 0.1	(7.71 ± 0.19) × 10^{-4}
	92.8 ± 0.1	(8.77 ± 0.23) × 10^{-4}
{CO_2-PVDF} sorption	3.0 ± 0.1	(3.10 ± 0.08) × 10^{-3}
	8.4 ± 0.1	(1.60 ± 0.04) × 10^{-3}
	13.3 ± 0.1	(6.19 ± 0.17) × 10^{-4}
	21.3 ± 0.1	(1.79 ± 0.05) × 10^{-4}
	29.6 ± 0.1	(3.84 ± 0.10) × 10^{-4}
	41.9 ± 0.1	(5.83 ± 0.16) × 10^{-4}
	53.8 ± 0.1	(6.55 ± 0.18) × 10^{-4}
	71.4 ± 0.1	(6.58 ± 0.18) × 10^{-4}
	94.2 ± 0.1	(6.73 ± 0.19) × 10^{-4}

TABLE VI
Global Cubic Thermal Expansion Coefficients $\alpha_{\text{pol-g-int}}$ at 372.02 K Obtained by Transitiometry with the Thermal II Differential with Reference Sample Mode during Pressurization under Either CO_2 or N_2 of MDPE and PVDF, Respectively

	P (MPa)	Global $\alpha_{\text{pol-g-int}}$ (K^{-1})
{CO_2–MDPE} sorption	2.8 ± 0.1	(1.08 ± 0.05) × 10^{-3}
	8.3 ± 0.1	(4.74 ± 0.10) × 10^{-4}
	16.2 ± 0.1	−(6.10 ± 0.14) × 10^{-5}
	22.3 ± 0.1	(9.84 ± 0.03) × 10^{-5}
	33.2 ± 0.1	(5.62 ± 0.11) × 10^{-4}
	40.7 ± 0.1	(7.54 ± 0.18) × 10^{-4}
	54.4 ± 0.1	(8.48 ± 0.15) × 10^{-4}
	68.2 ± 0.1	(9.20 ± 0.16) × 10^{-4}
	96.1 ± 0.1	(8.90 ± 0.12) × 10^{-4}
{CO_2–PVDF} sorption	3.2 ± 0.1	(2.20 ± 0.09) × 10^{-3}
	9.8 ± 0.1	(1.65 ± 0.04) × 10^{-3}
	16.3 ± 0.1	(5.08 ± 0.13) × 10^{-4}
	23.3 ± 0.1	(2.56 ± 0.06) × 10^{-4}
	31.2 ± 0.1	(4.04 ± 0.09) × 10^{-4}
	39.4 ± 0.1	(4.02 ± 0.09) × 10^{-4}
	50.8 ± 0.1	(5.39 ± 0.10) × 10^{-4}
	66.5 ± 0.1	(6.50 ± 0.11) × 10^{-4}
	89.7 ± 0.1	(6.43 ± 0.09) × 10^{-4}
{N_2–PVDF} sorption	2.9 ± 0.1	(9.62 ± 0.42) × 10^{-4}
	9.1 ± 0.1	(8.55 ± 0.22) × 10^{-4}
	15.9 ± 0.1	(8.47 ± 0.21) × 10^{-4}
	22.5 ± 0.1	(8.80 ± 0.22) × 10^{-4}
	30.8 ± 0.1	(8.40 ± 0.19) × 10^{-4}
	40.2 ± 0.1	(7.58 ± 0.16) × 10^{-4}
	51.6 ± 0.1	(8.20 ± 0.15) × 10^{-4}
	68.7 ± 0.1	(7.39 ± 0.11) × 10^{-4}
	92.0 ± 0.1	(7.35 ± 0.11) × 10^{-4}

TABLE VII
Global Cubic Thermal Expansion Coefficients $\alpha_{pol\text{-}g\text{-}int}$ at 372.02 K Obtained by Transitiometry with the Thermal II Differential with Reference Sample Mode during Depressurization under Either CO_2 or N_2 of PVDF

	P (MPa)	Global $\alpha_{pol\text{-}g\text{-}int}$ (K^{-1})
{CO_2–PVDF} desorption	90.1 ± 0.1	(7.12 ± 0.02) × 10^{-4}
	69.2 ± 0.1	(7.23 ± 0.04) × 10^{-4}
	52.2 ± 0.1	(7.00 ± 0.03) × 10^{-4}
	40.1 ± 0.1	(6.36 ± 0.01) × 10^{-4}
	30.8 ± 0.1	(4.94 ± 0.01) × 10^{-4}
	22.4 ± 0.1	(4.19 ± 0.01) × 10^{-4}
	15.7 ± 0.1	(1.03 ± 0.01) × 10^{-3}
	9.3 ± 0.1	(2.67 ± 0.01) × 10^{-3}
	3.1 ± 0.1	(2.79 ± 0.02) × 10^{-3}
{N_2–PVDF} desorption	92.8 ± 0.1	(7.07 ± 0.01) × 10^{-4}
	69.8 ± 0.1	(7.68 ± 0.04) × 10^{-4}
	52.5 ± 0.1	(8.07 ± 0.03) × 10^{-4}
	39.9 ± 0.1	(8.36 ± 0.02) × 10^{-4}
	30.3 ± 0.1	(8.31 ± 0.01) × 10^{-4}
	21.8 ± 0.1	(8.45 ± 0.01) × 10^{-4}
	15.0 ± 0.1	(9.40 ± 0.05) × 10^{-4}
	9.1 ± 0.1	(1.01 ± 0.01) × 10^{-3}
	2.8 ± 0.1	(9.71 ± 0.06) × 10^{-4}

under N_2 or Hg, that is, the isotherms of interaction vary ''monotonously'' (Fig. 8, bottom left-hand side). Below 30 MPa, more energetic interactions are observed with PVDF compared to MDPE, which is demonstrated by higher global $\alpha_{pol\text{-}g\text{-}int}$ {CO_2–PVDF}. Above 30 MPa, CO_2–MDPE interactions are larger than CO_2–PVDF interactions and the global $\alpha_{pol\text{-}g\text{-}int}$ for {CO_2–MDPE} system overpasses the global $\alpha_{pol\text{-}g\text{-}int}$ for {CO_2–PVDF} system. As shown in Figure 8 (bottom left-hand side and top right-hand side), in the case of PVDF, N_2 acts as a ''relatively neutral'' fluidlike Hg but with stronger interactions. The values with nitrogen are smaller than those with carbon dioxide [($\alpha_{pol\text{-}g\text{-}int}$ {N_2–PVDF} < $\alpha_{pol\text{-}g\text{-}int}$ {CO_2–PVDF}]: interactions of PVDF with N_2 appear weaker. With nitrogen—a relatively neutral fluid—the heat effects reflect the sorption under pressure; and parallels the remarkable plasticization efficiency of nitrogen in polystyrene, particularly at elevated pressure.[43] The PVDF values during decompression under N_2 and CO_2 are similar; what is satisfactory as regards the reversibility of the sorption/desorption phenomena.

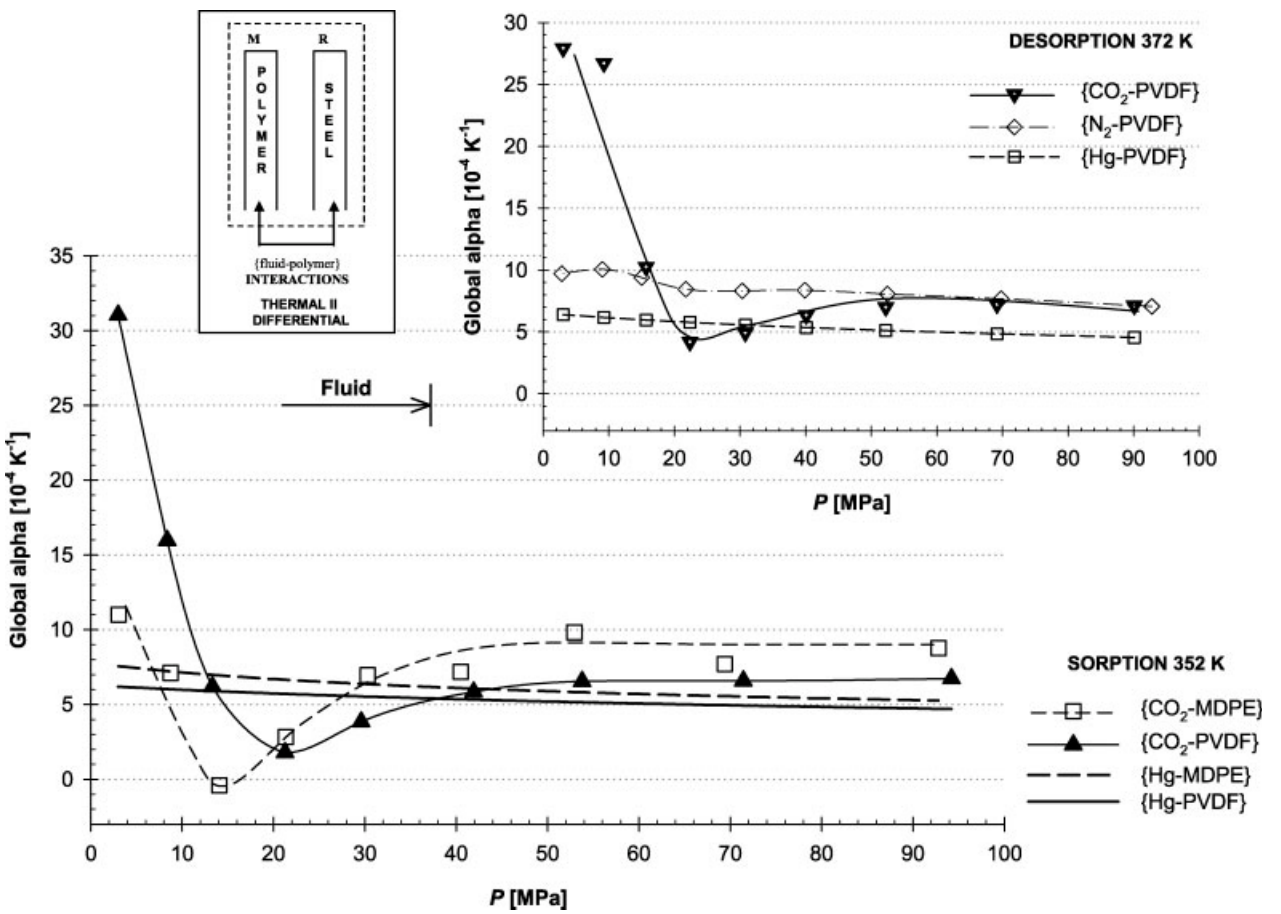

Figure 8 Global cubic thermal expansion coefficients $\alpha_{pol\text{-}g\text{-}int}$ at 352.38 and 372.02 K of MDPE and PVDF, under either CO_2 or N_2 or Hg during sorption and desorption under P jumps, obtained with the thermal II differential mode. The graphic on the top right-hand side shows the $\alpha_{pol\text{-}g\text{-}int}$ behavior of PVDF in presence of either CO_2 or N_2 compared to PVDF in presence of Hg (considered as an inert fluid).

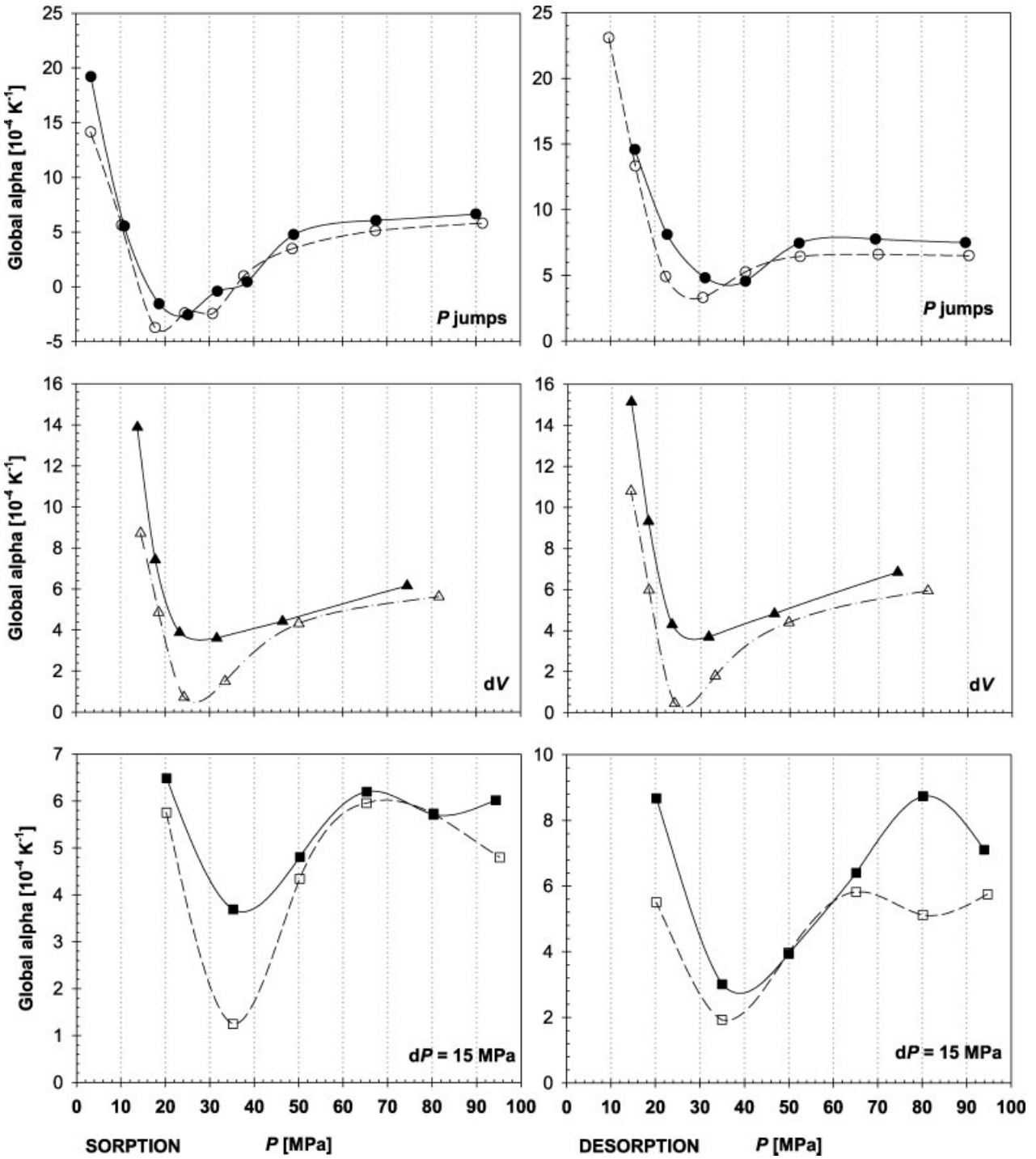

Figure 9 Comparison of global cubic thermal expansion coefficient $\alpha_{pol\text{-}g\text{-}int}$ of CO_2-PVDF at 401.50 K during either sorption or desorption under: P jumps, $dV = 1.364$ cm^3, and $dP = 15$ MPa, carried out with the thermal II differential mode. Two experiments are presented: the first with open symbols and the second with closed ones. The second run was carried out with PVDF samples previously saturated by CO_2 sorption under a 372.02 K isotherm.

The minimum of $\alpha_{pol\text{-}g\text{-}int}$ observed with {CO_2–MDPE} and {CO_2–PVDF} systems at about 15 MPa corresponds to the supercritical domain of CO_2. The dependency of $\alpha_{pol\text{-}g\text{-}int}$ coefficients with the nature of the pure gas, i.e., a minimum corresponding in a mirror-image to the maximum in the temperature dependence of α_p for pure CO_2 gas, is a striking feature of previous studies.[19] It clearly shows the influence of supercritical sorption on the thermophysical properties of the polymers. With the semicrystalline polymers, low pressures most probably induce a first adsorption of CO_2 in the amorphous part and in some

TABLE VIII
Global Cubic Thermal Expansion Coefficients $\alpha_{pol\text{-}g\text{-}int}$ at 401.50 K Obtained by Transitiometry with the Thermal II Differential with Reference Sample Mode during Pressurization under CO_2 of PVDF through Either *P* Jumps, or *V*, or *P* Scans (Experiment 1 and Experiment 2, Respectively)

{CO_2-PVDF}							
Experiment 1				Experiment 2			
Sorption		Desorption		Sorption		Desorption	
P (MPa)	Global $\alpha_{pol\text{-}g\text{-}int}$ (K^{-1})	*P* (MPa)	Global $\alpha_{pol\text{-}g\text{-}int}$ (K^{-1})	*P* (MPa)	Global $\alpha_{pol\text{-}g\text{-}int}$ (K^{-1})	*P* (MPa)	Global $\alpha_{pol\text{-}g\text{-}int}$ (K^{-1})
P jumps							
3.3 ± 0.1	$(1.41 \pm 0.06) \times 10^{-3}$	90.7 ± 0.1	$(6.49 \pm 0.02) \times 10^{-4}$	3.4 ± 0.1	$(1.92 \pm 0.08) \times 10^{-3}$	89.9 ± 0.1	$(7.49 \pm 0.03) \times 10^{-4}$
10.3 ± 0.1	$(5.62 \pm 0.14) \times 10^{-4}$	70.3 ± 0.1	$(6.60 \pm 0.03) \times 10^{-4}$	10.9 ± 0.1	$(5.55 \pm 0.13) \times 10^{-4}$	69.6 ± 0.1	$(7.75 \pm 0.04) \times 10^{-4}$
17.8 ± 0.1	$-(3.73 \pm 0.09) \times 10^{-4}$	52.7 ± 0.1	$(6.42 \pm 0.03) \times 10^{-4}$	18.7 ± 0.1	$-(1.56 \pm 0.03) \times 10^{-4}$	52.5 ± 0.1	$(7.45 \pm 0.03) \times 10^{-4}$
24.5 ± 0.1	$-(2.42 \pm 0.06) \times 10^{-4}$	40.4 ± 0.1	$(5.24 \pm 0.01) \times 10^{-4}$	25.2 ± 0.1	$-(2.57 \pm 0.06) \times 10^{-4}$	40.4 ± 0.1	$(4.55 \pm 0.01) \times 10^{-4}$
30.8 ± 0.1	$-(2.45 \pm 0.06) \times 10^{-4}$	30.8 ± 0.1	$(3.30 \pm 0.01) \times 10^{-4}$	31.8 ± 0.1	$-(4.13 \pm 0.10) \times 10^{-5}$	31.3 ± 0.1	$(4.81 \pm 0.01) \times 10^{-4}$
37.8 ± 0.1	$(9.83 \pm 0.24) \times 10^{-5}$	22.4 ± 0.1	$(4.92 \pm 0.01) \times 10^{-4}$	38.5 ± 0.1	$(4.37 \pm 0.11) \times 10^{-5}$	22.8 ± 0.1	$(8.11 \pm 0.01) \times 10^{-4}$
48.7 ± 0.1	$(3.48 \pm 0.07) \times 10^{-4}$	15.6 ± 0.1	$(1.33 \pm 0.01) \times 10^{-3}$	49.0 ± 0.1	$(4.76 \pm 0.09) \times 10^{-4}$	15.5 ± 0.1	$(1.46 \pm 0.01) \times 10^{-3}$
67.4 ± 0.1	$(5.11 \pm 0.08) \times 10^{-4}$	9.6 ± 0.1	$(2.31 \pm 0.02) \times 10^{-3}$	67.5 ± 0.1	$(6.06 \pm 0.09) \times 10^{-4}$		
91.5 ± 0.1	$(5.80 \pm 0.08) \times 10^{-4}$			90.0 ± 0.1	$(6.64 \pm 0.10) \times 10^{-4}$		
Volume variation *dV* (steps)							
14.5 ± 0.1	$(8.72 \pm 0.15) \times 10^{-4}$	81.1 ± 0.1	$(5.93 \pm 0.07) \times 10^{-4}$	13.8 ± 0.1	$(1.39 \pm 0.02) \times 10^{-3}$	74.3 ± 0.1	$(6.85 \pm 0.08) \times 10^{-4}$
18.6 ± 0.1	$(4.86 \pm 0.16) \times 10^{-4}$	49.8 ± 0.1	$(4.39 \pm 0.03) \times 10^{-4}$	17.8 ± 0.1	$(7.42 \pm 0.26) \times 10^{-4}$	46.6 ± 0.1	$(4.82 \pm 0.03) \times 10^{-4}$
24.3 ± 0.1	$(7.29 \pm 0.20) \times 10^{-5}$	33.2 ± 0.1	$(1.79 \pm 0.01) \times 10^{-4}$	23.3 ± 0.1	$(3.88 \pm 0.11) \times 10^{-4}$	31.8 ± 0.1	$(3.69 \pm 0.01) \times 10^{-4}$
33.5 ± 0.1	$(1.50 \pm 0.03) \times 10^{-4}$	24.1 ± 0.1	$(4.51 \pm 0.01) \times 10^{-5}$	31.7 ± 0.1	$(3.60 \pm 0.08) \times 10^{-4}$	23.5 ± 0.1	$(4.29 \pm 0.01) \times 10^{-4}$
50.1 ± 0.1	$(4.32 \pm 0.07) \times 10^{-4}$	18.3 ± 0.1	$(5.97 \pm 0.04) \times 10^{-4}$	46.5 ± 0.1	$(4.43 \pm 0.07) \times 10^{-4}$	18.2 ± 0.1	$(9.32 \pm 0.08) \times 10^{-4}$
81.6 ± 0.1	$(5.63 \pm 0.07) \times 10^{-4}$	14.3 ± 0.1	$(1.08 \pm 0.02) \times 10^{-3}$	74.5 ± 0.1	$(6.16 \pm 0.08) \times 10^{-4}$	14.4 ± 0.1	$(1.51 \pm 0.02) \times 10^{-3}$
Pressure variation $dP = 15$ MPa (steps)							
20.2 ± 0.1	$(5.75 \pm 0.09) \times 10^{-4}$	94.7 ± 0.1	$(5.75 \pm 0.06) \times 10^{-4}$	20.3 ± 0.1	$(6.49 \pm 0.10) \times 10^{-4}$	94.0 ± 0.1	$(7.10 \pm 0.08) \times 10^{-4}$
35.2 ± 0.1	$(1.25 \pm 0.02) \times 10^{-4}$	80.1 ± 0.1	$(5.12 \pm 0.02) \times 10^{-4}$	35.3 ± 0.1	$(3.69 \pm 0.06) \times 10^{-4}$	80.2 ± 0.1	$(8.73 \pm 0.02) \times 10^{-4}$
50.3 ± 0.1	$(4.34 \pm 0.07) \times 10^{-4}$	65.2 ± 0.1	$(5.82 \pm 0.02) \times 10^{-4}$	50.3 ± 0.1	$(4.81 \pm 0.08) \times 10^{-4}$	65.2 ± 0.1	$(6.40 \pm 0.02) \times 10^{-4}$
65.3 ± 0.1	$(5.96 \pm 0.10) \times 10^{-4}$	50.0 ± 0.1	$(3.97 \pm 0.01) \times 10^{-4}$	65.3 ± 0.1	$(6.20 \pm 0.10) \times 10^{-4}$	50.0 ± 0.1	$(3.94 \pm 0.01) \times 10^{-4}$
80.3 ± 0.1	$(5.73 \pm 0.10) \times 10^{-4}$	35.0 ± 0.1	$(1.92 \pm 0.01) \times 10^{-4}$	80.3 ± 0.1	$(5.71 \pm 0.10) \times 10^{-4}$	35.0 ± 0.1	$(3.01 \pm 0.01) \times 10^{-4}$
95.2 ± 0.1	$(4.80 \pm 0.08) \times 10^{-4}$	20.2 ± 0.1	$(5.50 \pm 0.02) \times 10^{-4}$	94.4 ± 0.1	$(6.02 \pm 0.10) \times 10^{-4}$	20.2 ± 0.1	$(8.67 \pm 0.03) \times 10^{-4}$

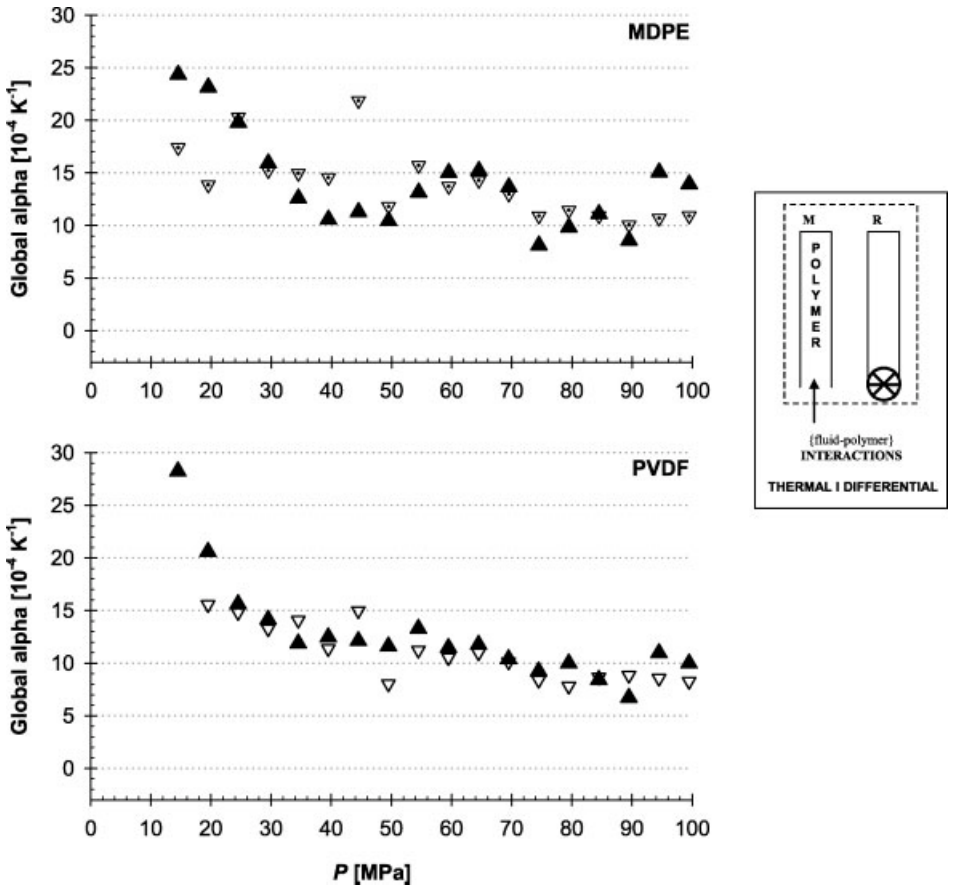

Figure 10 Comparison of global cubic thermal expansion coefficients $\alpha_{pol\text{-}g\text{-}int}$ between {CO_2-MDPE} and {CO_2-PVDF} systems at 373.40 K along P scans $dP = 5$ MPa, obtained with the thermal I differential mode. Closed and open symbols correspond respectively, to sorption and desorption runs.

interstitial sites of the crystalline part with the possible formation of a micro-organized domain generated in the amorphous phase of the polymer.[44] High pressures favor the absorption into the whole polymer matrix, i.e., deeply inside the interstitial or other voids in the polymer, with a mechanical distension, in such a way that the CO_2-saturated polymer behaves as a pseudohomogeneous phase.[18]

Furthermore, the minimum would mean that supercritical gas–polymer interactions are favored. The lowering of molecular polymer–polymer interactions is concomitantly associated to the easiness of CO_2 dissolution into the polymer matrix inducing thus an increase of free volume together with an increase in polymer chain mobility.[45] This plasticization effect is shown by the minimum of $\alpha_{pol\text{-}g\text{-}int}$ as function of pressure. Quantitatively, this is confirmed by the net increase of gas sorption into the polymer and the swelling of the polymer due to the sorption around 15 MPa (as investigated by the gravimetric–volumetric VW-*PVT* method).[1,11,39] As a matter of fact, around this pressure, there is compensation between plasticization and hydrostatic pressure effects upon high CO_2-pressure sorption into the polymer. The supercritic-hydrostatic pressure corresponding to the minimum for MDPE is slightly smaller than that of PVDF.

The thermal II differential mode with reference sample: PVDF at 402 K under P jumps and (P, V) scanning modes

Isothermal and dynamic measurements under pressure jumps during different volume and pressure scans were studied in more details. Other experiments with PVDF samples already modified during 372.02 K isotherms were conducted. Series of measurements dealt with the {CO_2–PVDF} system at 401.50 K using two types of scanning modes: volume scanning mode with a change of the calorimetric active volume of $dV = 1.364$ cm^3 (with a scanning rate of about 11×10^{-4} cm^3 s^{-1}) and pressure scanning mode with a change of the pressure $dP = 15$ MPa (with a scanning rate of about 45×10^{-4} MPa s^{-1}). The investigated pressure range was from 0.1 to 100 MPa. The experimental heats measured as function of volume and of pressure show shallow minimums in the 20–40 MPa region.

TABLE IX
Global Cubic Thermal Expansion Coefficients $\alpha_{pol\text{-}g\text{-}int}$ at 373.40 K Obtained by Transitiometry with the Thermal I Differential without Reference Mode during Pressurization under CO_2 of MDPE and PVDF, Respectively with Pressure Scans $dP = 5$ MPa at 45×10^{-4} MPa s^{-1}

{CO_2-MDPE}				{CO_2-PVDF}			
Sorption		Desorption		Sorption		Desorption	
P (MPa)	Global $\alpha_{pol\text{-}g\text{-}int}$ (K^{-1})	P (MPa)	Global $\alpha_{pol\text{-}g\text{-}int}$ (K^{-1})	P (MPa)	Global $\alpha_{pol\text{-}g\text{-}int}$ (K^{-1})	P (MPa)	Global $\alpha_{pol\text{-}g\text{-}int}$ (K^{-1})
14.5 ± 0.1	$(2.43 \pm 0.04) \times 10^{-3}$	99.5 ± 0.1	$(1.09 \pm 0.01) \times 10^{-3}$	14.5 ± 0.1	$(2.82 \pm 0.05) \times 10^{-3}$	99.5 ± 0.1	$(8.27 \pm 0.09) \times 10^{-4}$
19.5 ± 0.1	$(2.31 \pm 0.07) \times 10^{-3}$	94.5 ± 0.1	$(1.07 \pm 0.01) \times 10^{-3}$	19.5 ± 0.1	$(2.06 \pm 0.06) \times 10^{-3}$	94.5 ± 0.1	$(8.57 \pm 0.09) \times 10^{-4}$
24.5 ± 0.1	$(1.98 \pm 0.06) \times 10^{-3}$	89.5 ± 0.1	$(1.00 \pm 0.01) \times 10^{-3}$	24.5 ± 0.1	$(1.56 \pm 0.05) \times 10^{-3}$	89.5 ± 0.1	$(8.83 \pm 0.09) \times 10^{-4}$
29.5 ± 0.1	$(1.59 \pm 0.05) \times 10^{-3}$	84.5 ± 0.1	$(1.09 \pm 0.01) \times 10^{-3}$	29.5 ± 0.1	$(1.41 \pm 0.04) \times 10^{-3}$	84.5 ± 0.1	$(8.67 \pm 0.09) \times 10^{-4}$
34.5 ± 0.1	$(1.26 \pm 0.04) \times 10^{-3}$	79.5 ± 0.1	$(1.14 \pm 0.01) \times 10^{-3}$	34.5 ± 0.1	$(1.19 \pm 0.03) \times 10^{-3}$	79.5 ± 0.1	$(7.80 \pm 0.08) \times 10^{-4}$
39.5 ± 0.1	$(1.06 \pm 0.03) \times 10^{-3}$	74.5 ± 0.1	$(1.09 \pm 0.01) \times 10^{-3}$	39.5 ± 0.1	$(1.25 \pm 0.04) \times 10^{-3}$	74.5 ± 0.1	$(8.37 \pm 0.08) \times 10^{-4}$
44.5 ± 0.1	$(1.13 \pm 0.03) \times 10^{-3}$	69.5 ± 0.1	$(1.30 \pm 0.01) \times 10^{-3}$	44.5 ± 0.1	$(1.21 \pm 0.04) \times 10^{-3}$	69.5 ± 0.1	$(1.01 \pm 0.01) \times 10^{-3}$
49.5 ± 0.1	$(1.04 \pm 0.03) \times 10^{-3}$	64.5 ± 0.1	$(1.43 \pm 0.01) \times 10^{-3}$	49.5 ± 0.1	$(1.16 \pm 0.03) \times 10^{-3}$	64.5 ± 0.1	$(1.10 \pm 0.01) \times 10^{-3}$
54.5 ± 0.1	$(1.31 \pm 0.04) \times 10^{-3}$	59.5 ± 0.1	$(1.37 \pm 0.01) \times 10^{-3}$	54.5 ± 0.1	$(1.33 \pm 0.04) \times 10^{-3}$	59.5 ± 0.1	$(1.05 \pm 0.01) \times 10^{-3}$
59.5 ± 0.1	$(1.50 \pm 0.05) \times 10^{-3}$	54.5 ± 0.1	$(1.57 \pm 0.02) \times 10^{-3}$	59.5 ± 0.1	$(1.15 \pm 0.03) \times 10^{-3}$	54.5 ± 0.1	$(1.12 \pm 0.01) \times 10^{-3}$
64.5 ± 0.1	$(1.52 \pm 0.04) \times 10^{-3}$	49.5 ± 0.1	$(1.18 \pm 0.01) \times 10^{-3}$	64.5 ± 0.1	$(1.18 \pm 0.04) \times 10^{-3}$	49.5 ± 0.1	$(8.03 \pm 0.08) \times 10^{-4}$
69.5 ± 0.1	$(1.36 \pm 0.04) \times 10^{-3}$	44.5 ± 0.1	$(2.19 \pm 0.02) \times 10^{-3}$	69.5 ± 0.1	$(1.04 \pm 0.03) \times 10^{-3}$	44.5 ± 0.1	$(1.50 \pm 0.02) \times 10^{-3}$
74.5 ± 0.1	$(8.11 \pm 0.24) \times 10^{-4}$	39.5 ± 0.1	$(1.46 \pm 0.01) \times 10^{-3}$	74.5 ± 0.1	$(9.22 \pm 0.28) \times 10^{-4}$	39.5 ± 0.1	$(1.14 \pm 0.09) \times 10^{-3}$
79.5 ± 0.1	$(9.83 \pm 0.29) \times 10^{-4}$	34.5 ± 0.1	$(1.50 \pm 0.02) \times 10^{-3}$	79.5 ± 0.1	$(9.98 \pm 0.29) \times 10^{-4}$	34.5 ± 0.1	$(1.41 \pm 0.01) \times 10^{-3}$
84.5 ± 0.1	$(1.11 \pm 0.03) \times 10^{-3}$	29.5 ± 0.1	$(1.52 \pm 0.02) \times 10^{-3}$	84.5 ± 0.1	$(8.42 \pm 0.25) \times 10^{-4}$	29.5 ± 0.1	$(1.32 \pm 0.01) \times 10^{-3}$
89.5 ± 0.1	$(8.58 \pm 0.26) \times 10^{-4}$	24.5 ± 0.1	$(2.03 \pm 0.02) \times 10^{-3}$	89.5 ± 0.1	$(6.72 \pm 0.20) \times 10^{-4}$	24.5 ± 0.1	$(1.48 \pm 0.01) \times 10^{-3}$
94.5 ± 0.1	$(1.51 \pm 0.05) \times 10^{-3}$	19.5 ± 0.1	$(1.39 \pm 0.01) \times 10^{-3}$	94.5 ± 0.1	$(1.10 \pm 0.03) \times 10^{-3}$	19.5 ± 0.1	$(1.56 \pm 0.02) \times 10^{-3}$
99.5 ± 0.1	$(1.39 \pm 0.04) \times 10^{-3}$	14.5 ± 0.1	$(1.74 \pm 0.02) \times 10^{-3}$	99.5 ± 0.1	$(9.97 \pm 0.03) \times 10^{-4}$		

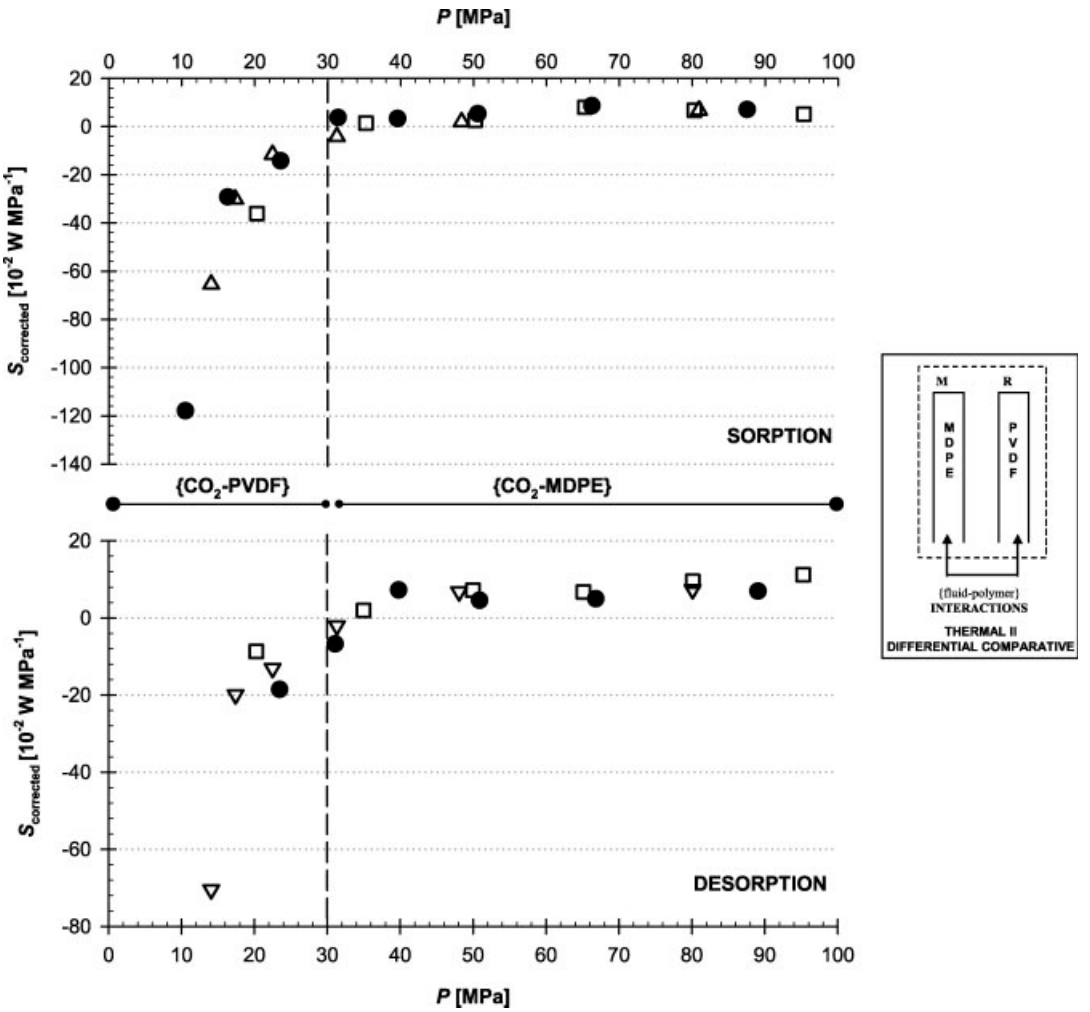

Figure 11 Differential heat flux observed when two polymers, MDPE and PVDF, are submitted to CO_2 at 372.59 K, with the thermal II differential comparative mode. Pressure domains showing the trend of heat fluxes for both polymers along either sorption or desorption under: P jumps (closed circles), volume changes $dV = 1.364$ cm^3 (open triangles), and pressure changes d$P = 15$ MPa (open squares), respectively.

Figure 9 (see data listed in Table VIII) shows not only the variations of $\alpha_{\text{pol-g-int}}$ of PVDF polymer during P jumps but also the evolution of the thermal expansion of the polymer during either P or V scans. Results for P or V scans are similar and show a good reproducibility with a slight shift of the minimum between 15 and 30 MPa. The differences are more marked with P jumps.

The uncertainties may be essentially due to the manner with which the pressure changes are transmitted to the investigated samples. During fast compression, the system is thermodynamically off balance, whereas transitiometry is a technique that yields optimal response at the thermodynamic equilibrium, where Maxwell relations can apply. Most likely, the small shift of the minimum toward higher pressures in the case of V scans compared to P jumps would be a consequence of the relaxation of the system, which reaches a more stable state under thermodynamic equilibrium.

The thermal I differential without reference sample

This part was devoted to the study of interactions using the thermal I differential mode. As previously, the variations of calorimetric signal were directly proportional to the differential heat flux due to gas–polymer interactions in the measuring cell during pressure changes. Only interactions at 373.40 K were investigated with MDPE and PVDF during a change in pressure $dP = 5$ MPa with a scanning rate of about 45 $\times 10^{-4}$ MPa s^{-1} (Fig. 10, Table IX). Interactions were investigated during sorption and desorption in the pressure range of 14–100 MPa; the obtained calorimetric signal passes through a shallow minimum at about 37–42 MPa.

As seen above, thermal coefficients with the thermal II differential mode pass through a minimum around 18 MPa for MDPE and 25 MPa for PVDF; results with thermal I differential mode would confirm then the previous observations made with the thermal II differential mode. However, the minimum between 10 and 30 MPa is less marked, and appears at higher pressure, around 40 MPa for MDPE and around 35 MPa for PVDF. This would suggest that the former differential mode allows more sensitive detection.

Conclusion: The thermal II differential comparative mode

To confirm the observed trends, a new and original thermal II differential comparative mode was experimented in measuring the differential heat flux obtained when a MDPE and a PVDF sample (of identical size and volume, each placed in one of the two calorimetric cells) are simultaneously submitted to the same gas pressure at an identical temperature (372.59 K). The experimental signal compares directly the interactions of the two polymers in the same gas/supercritical environment at constant temperature. The calorimetric responses were collected during pressures jumps and during continuous volume and pressure scans (Fig. 11).

Below 30 MPa, calorimetric signals are endothermic, with $dQ(\text{MDPE–PVDF})/dP < 0$, i.e., the PVDF exhibits higher interactions with CO_2 than MDPE. Above 30 MPa, calorimetric signals become exothermic with $dQ(\text{MDPE–PVDF})/dP > 0$, i.e., the differential heat flux of interactions for the {CO_2–MDPE} system becomes larger than that for the {CO_2–PVDF} system (Table X).

This direct comparative method, which permits to differentiate the interactions between both polymers (MDPE and PVDF) submitted to the same supercritical CO_2 pressure, reproduces exactly the results obtained with the two preceding methods. At low pressures more energetic interactions are observed with PVDF compared to MDPE. Both polymers having the same degree of crystallinity X_c of about 50%, the high energy can be favored by the presence of fluoride in pure PVDF, i.e., the strong and high polar C—F bonds can give high dipolar interactions with the polarizable CO_2.[41] These interactions are stronger than the interactions between the chains segments. Then larger energetic interactions of PVDF may suggest that incorporation of CO_2 in PVDF is stronger than that in MDPE, which was confirmed with the experiments of sorption and of swelling using VW-*PVT*. In addition, this is somewhat confirmed by measurements at high pressure, which show that thermal expansion coefficients are smaller for highly condensed {CO_2–PVDF} systems than that for less condensed {CO_2–MDPE} systems. Effectively as shown in Figure 8, at high pressure, say above 30 MPa, the global cubic thermal expansion coefficient is smaller for {CO_2–PVDF} (for which the gas–polymer interactions are larger) than that for {CO_2–MDPE}.

TABLE X
Dependence of the "Interaction" Heat Flux with the Type of Polymer Submitted to High CO_2 Pressure

Heat flux	Low pressures < 30 MPa	High pressures > 30 MPa
Evolution of the signal under CO_2	↘	↗
MDPE	−	+
PVDF	+	−

CONCLUSIONS

This contribution reviews most of the recent data obtained to study gas–polymer interactions of two thermoplastic semicrystalline polymers MDPE and PVDF, between T_g and T_m, with either CO_2 or N_2. The trends characterizing gas solubility and swelling of the polymers during sorption and the associated energy of interactions obtained through different techniques are self consistent. The vibrating-wire sensor (VW-*PVT*) has been used for the evaluation of the concentration *C* of CO_2 in (MDPE and PVDF). The swelling of the polymer due to the sorption effect was calculated and obtained by applying the SL model. Scanning transitiometry (PCSC) has been used for the evaluation of the global cubic expansion coefficients $\alpha_{\text{pol-g-int}}$ of MDPE and PVDF saturated with supercritical gas (CO_2 or N_2). Detections thermal II differential mode with reference sample and thermal I differential mode without reference sample were used as well as a thermal II differential comparative mode. Results show satisfactory agreement for experiments obtained either during *P* jumps or step-wise *dV* or *dP* scans.

For both experimental techniques, data obtained during gas sorption or desorption along isotherms do not show significant hysteresis. The larger effect of CO_2 on gas–polymer interactions is located in the range of 15–25 MPa, where competition takes place between plasticization effect and hydrostatic fluid effect. This means that gas absorption into the polymer and concomitant swelling are favored in the vicinity of the critical region of CO_2; simultaneously and accordingly, the heat of interaction increases after passing through a minimum.

This research work was proposed by the "Institut Français du Pétrole" (IFP) Lyon. Recommendations for experimental measurements expressed by S. L. Randzio (Institute of Physical Chemistry, Polish Academy of Sciences, Warsaw, Poland) and by F. Dan (Department of Macromolecular Chemistry, Gh. Asachi Technical University, Iasi, Romania) are highly appreciated.

References

1. Boyer, S. A. E.; Grolier, J.-P. E. Polymer 2005, 46, 3737.
2. Dewimille, B.; Martin, J.; Jarrin, J. J de Physique IV 1993, 3, 1559.
3. Jarrin, J.; Dewimille, B.; Devaux, E.; Martin, J. Int SPE 1994, 28482, 203.
4. Von Solms, N.; Zecchin, N.; Rubin, A.; Andersen, S. I.; Stenby, E. H. Eur Polym J 2005, 41, 341.
5. Klopffer, M.-H.; Flaconnèche, B. Oil Gas Sci Technol Rev IFP 2001, 56, 223.
6. Flaconnèche, B.; Martin, J.; Klopffer, M.-H. Oil Gas Sci Technol Rev IFP 2001, 56, 245.
7. Flaconnèche, B.; Martin, J.; Klopffer, M.-H. Oil Gas Sci Technol Rev IFP 2001, 56, 261.
8. Scheichl, R.; Klopffer, M.-H.; Benjelloun-Dabaghi, Z.; Flaconnèche, B. J Membr Sci 2005, 254, 275.
9. Kamiya, Y.; Hirose, T.; Mizoguchi, K.; Naito, Y. J Polym Sci Part B: Polym Phys 1986, 24, 1525.
10. Chaudary, B. I.; Johns, A. I. J Cell Plast 1998, 34, 312.
11. Sato, Y.; Fujiwara, K.; Takikawa, T.; Sumarno; Takishima, S.; Masuoka, H. Fluid Phase Equilib 1999, 162, 261.
12. Miller-Chou, B. A.; Koenig, J. L. Prog Polym Sci 2003, 28, 1223.
13. Duarte, A. R. C.; Anderson, L. E.; Duarte, C. M. M.; Kazarian, S. G. J Supercrit Fluids 2005, 36, 160.
14. Pantoula, M.; Panayiotou, C. J Supercrit Fluids 2006, 37, 254.
15. Hilic, S.; Pádua, A. A. H.; Grolier, J.-P. E. Rev Sci Instrum 2000, 71, 4236.
16. Hilic, S.; Boyer, S. A. E.; Pádua, A. A. H.; Grolier, J.–P. E. J Polym Sci Part B: Polym Phys 2001, 39, 2063.
17. Grolier, J.-P. E. Pure Appl Chem 2005, 77, 1297.
18. Boyer, S. A. E.; Randzio, S. L.; Grolier, J.-P. E. J Polym Sci Part B: Polym Phys 2006, 44, 185.
19. Grolier, J.-P. E.; Dan, F.; Boyer, S. A. E.; Orlowska, M.; Randzio, S. L. Int J Thermophys 2004, 25, 297.
20. Sanchez, I. C.; Lacombe, R. H. Macromolecules 1978, 11, 1145.
21. Boudouris, D.; Constantinou, L.; Panayiotou, C. Fluid Phase Equilib 2000, 167, 1.
22. Hariharan, R.; Freeman, B. D.; Carbonell, R. G.; Sarti, G. C. J Appl Polym Sci 1993, 50, 1781.
23. DeAngelis, M. G.; Merkel, T. C.; Bondar, V. I.; Freeman, B. D.; Doghieri, F.; Sarti, G. C. J Polym Sci Part B: Polym Phys 1999, 37, 3011.
24. Randzio, S. L. Thermochim Acta 1997, 300, 29.
25. Randzio, S. L. Thermochim Acta 2000, 355, 107.
26. Flaconnèche, B.; Martin, J.; Klopffer, M.-H. Private communication. Data obtained at IFP 2001.
27. Bazourdy, E.; Martin, J. Etude de l'influence du confinement sur le comportement de matériaux polymères soumis à de fortes pressions de gaz, IFP internal report; IFP: France, 1999.
28. Meares, P. J Am Chem Soc 1954, 76, 3415.
29. Barrer, R. M.; Barrie, J. A.; Slater, J. J Polym Sci 1958, 27, 177.
30. Michaels, A. S.; Bixler, H. J. J Polym Sci 1961, 50, 393.
31. Vieth, W. R.; Sladek, K. J. J Colloïd Sci 1965, 20, 1014.
32. Vieth, W. R.; Tam, P. M.; Michaels, A. S. J Colloïd Interface Sci 1966, 22, 360.
33. Vieth, W. R.; Howell, J. M.; Hsieh, J. H. J Membr Sci 1976, 1, 177.
34. Koros, W. J.; Paul, D. R. J Polym Sci Polym Phys Ed 1978, 16, 1947.
35. Banerjee, T.; Lipscomb, G. G. Comput Theor Polym Sci 2000, 10, 437.
36. Tsujita, Y. Prog Polym Sci 2003, 28, 1377.
37. Hu, C.-C.; Chang, C.-S.; Ruaan, R.-C.; Lai, J.-Y. J Membr Sci 2003, 226, 51.
38. Rodgers, P. Equation-of-State predictions of solubility in semicrystalline poly(vinylidene fluoride), IFP internal report; IFP: France, 1992.
39. Lorge, O.; Briscoe, B. J.; Dang, P. Polymer 1999, 40, 2981.
40. Ghosal, K.; Chern, R. T.; Freeman, B. D.; Savariar, R. J Polym Sci Part B: Polym Phys 1995, 33, 657.
41. Bos, A.; Pünt, I. G. M.; Wessling, M.; Strathmann, H. J Membr Sci 1999, 155, 67.
42. Hansen, A. R.; Eckert, C. A. J Chem Eng Data 1991, 36, 252.
43. Boyer, S. A. E.; Grolier, J.-P. E. Pure Appl Chem 2005, 77, 593.
44. Mogri, Z.; Paul, D. R. Polymer 2001, 42, 7781.
45. Ismail, A. F.; Lorna, W. Sep Purif Technol 2002, 27, 173.